Appl. Phys. B 71, 747–753 (2000) / Digital Object Identifier (DOI) 10.1007/s003400000454

Applied Physics B
Lasers
and Optics

Optical tweezers for confocal microscopy

A. Hoffmann*, G. Meyer zu Hörste, G. Pilarczyk, S. Monajembashi, V. Uhl, K.O. Greulich

Institut für Molekulare Biotechnologie e.V. (IMB), Abt. Einzelzell- und Einzelmolekültechniken, Beutenbergstrasse 11, 07745 Jena, Germany
(Fax: +49-3641/656-410, E-mail: hoan@imb-jena.de)

Received: 24 March 2000/Revised version: 23 June 2000/Published online: 11 October 2000 –

Abstract. In confocal laser scanning microscopes (CLSMs), lasers can be used for image formation as well as tools for the manipulation of microscopic objects. In the latter case, in addition to the imaging lasers, the light of an extra laser has to be focused into the object plane of the CLSM, for example as optical tweezers. Imaging as well as trapping by optical tweezers can be done using the same objective lens. In this case, *z*-sectioning for 3D imaging shifts the optical tweezers with the focal plane of the objective along the optical axis, so that a trapped object remains positioned in the focal plane. Consequently, 3D imaging of trapped objects is impossible without further measures. We present an experimental set-up keeping the axial trapping position of the optical tweezers at its intended position whilst the focal plane can be axially shifted over a distance of about 15 μm. It is based on fast-moving correctional optics synchronized with the objective movement. First examples of application are the 3D imaging of chloroplasts of Elodea densa (Canadian waterweed) in a vigorous cytoplasmic streaming and the displacement of zymogen granules in pancreatic cancer cells (AR42 J).

PACS: 87.64.-t; 87.16.-b

Laser light can be easily focused into a spot of submicrometer dimensions in a microscope. When an object is transparent for a given wavelength, even focusing into the object's interior is possible. Since light is a carrier of energy that may be converted into heat, high temperatures up to nanoplasmas can be induced in the laser-light focus. Since, in addition, light is a carrier of momentum, forces can be exerted too. This has been exploited in conventional microscopes to use laser light first for submicrometer machining with laser microbeams, see for example [1–3], and then for complete micromanipulation by light with microbeams and optical tweezers in conventional microscopes [4–6]. Within the last few years the use of optical tweezers for photonic force microscopy opened up new field of applications with optical tweezers [7].

*Corresponding author.

Optical tweezers are based on forces due to radiation pressure, with the gradient force as dominant force component [8]. The gradient force pulls dielectric particles into the high-intensity gradient region of an infrared laser beam focused by an objective with high numerical aperture. Thus, optical forces can be used to fix and move dielectric particles and furthermore to precisely measure forces in the piconewton range [9–11]. Optical tweezers have now been widely used in biology and physics. They offer the opportunity for subcellular manipulation and studying cellular processes that require precise positioning of cell organelles [12]. Examples include the manipulation of cell nuclei as well as organelles in plant cells and the displacement of chromosomes [13–15].

Confocal laser scanning microscopes (CLSMs) assemble a number of two-dimensional optical sections to finally reconstitute a three-dimensional image (*z*-sectioning). Using these sectioning capabilities combined with the 3D-manipulation possibilities of the optical tweezers, CLSMs are excellent imaging tools for 3D micromanipulation [16, 17]. Particularly in CLSMs, where the scan time per frame is of the order of seconds, optical tweezers can alleviate the serious problem of motional blurring of moving objects by spatially fixing them, even inside living cells.

So far, attempts to use laser microtools in CLSMs have been only moderately successful. When imaging as well as trapping by optical tweezers are done using the same objective lens, a conflict arises between the 3D imaging and the axial positioning of the focus of the laser used for optical tweezers [17]: whenever the microscope objective is moved along the optical axis for *z*-sectioning, the focus of the optical tweezers is shifted with the focal plane of the objective. So a trapped object remains positioned in focus while its former surroundings go into defocus. Consequently, 3D imaging of trapped objects as well as imaging of a trapped object in its surroundings for 3D-position detection are impossible without further measures. In the following we present a new experimental set-up keeping the trapping position of the optical tweezers at its intended position whilst the focal plane can be axially shifted, allowing 3D imaging of trapped objects.

As a first example confocal imaging of chloroplasts in leaf cells of Elodea densa (Canadian waterweed) possess-

ing a vigorous cytoplasmic streaming is shown. Furthermore, a perspective for an application with pancreatic cancer cells (AR42 J) is given.

1 Materials and methods

1.1 Experimental set-up

The experimental set-up is based on an inverted confocal laser scanning microscope (LSM 510, Carl Zeiss Jena GmbH, Jena, Germany) equipped with an argon-ion laser (458 nm, 488 nm) and a green HeNe laser (543 nm) as scanning lasers. The LSM 510 carries out *z*-sectioning for 3D imaging by moving the objective along the optical axis (*z*-direction) in order to scan optical sections of an object at different *z*-positions.

In our experimental set-up (shown in Fig. 1a) a Nd:YAG laser (1064 nm, max. power 11 W; T40-Z-106C, Spectra Physics, Darmstadt, Germany) running in cw mode is used for the optical tweezers. A single-mode fiber (BTO Bungert GmbH, Weil der Stadt, Germany) directs the laser light from the Nd:YAG laser to the rear side of the microscope. The fiber output efficiency with the single-mode fiber coupler used (THORLABS, Grünberg, Germany) is about 60%. The fiber end is fixed on a translation stage ("TS" in Fig. 1a) that can be displaced in the axial direction. The stage has a travel length of 10 mm (LINOS Photonics GmbH, Göttingen, Germany) and is equipped with a stepper motor (MOVTEC Stütz & Wacht GmbH, Pforzheim, Germany). The motor is adjusted to 2000 steps/revolution, resulting in a stage shift of 250 nm/step, a maximum velocity of 10 000 steps/s, and an acceleration of 20 000 steps/s^2. A convex lens ("L", $f = 40$ mm), added externally into the path of the laser beam, focuses the light emerging from the fiber into the epi-fluorescence illumination path ("FIP") where another convex lens ($f = 150$ mm) is located. The single-mode fiber together with the external lens present a suitable beam expander, because of the divergence of the beam emerging from the fiber, reducing the number of optical elements required for an adequate expansion of the laser beam. Finally, the dichroic mirrors located in the fluorescence reflector slide ("FRS") direct the laser light to the back aperture of the objective ("O") that has to be entirely illuminated by the infrared laser light to obtain an almost diffraction-limited beam for good trapping efficiency [6, 18]. For this purpose, the existing mirrors for epi-fluorescence illumination are replaced by mirrors being additionally reflective for the infrared laser light used for the optical tweezers (AHF Analysentechnik, Tübingen, Germany). For the use of the optical tweezers in laser scanning mode, yet another dielectric mirror (Laser Optik GmbH, Garbsen, Germany) is placed on the laser scanning position of the fluorescence reflector slide that otherwise would be empty. It reflects the infrared laser light and is simultaneously transparent for the scanning lasers coming from below and the emitted fluorescence. Hence, the complete imaging capabilities of the original LSM 510 are maintained.

For the determination of the relative objective position, internal signals controlling the motor that shifts the microscope objective are registered. This registration is carried out by a PC equipped with a data-acquisition board and a stepper board (PCI-6023E and PCI-Step-20X, National Instruments, München, Germany) that is used for controlling the stepper-motor position of the translation stage. A program routine developed with the software LabVIEW 5.1 (National Instruments, München, Germany) controls the signal registration and determines the relative objective position. Mediated by a calibration curve (see results and Sect. 1.2), this program simultaneously calculates and controls the stage position as a function of the relative objective position, as illustrated in Fig. 1b.

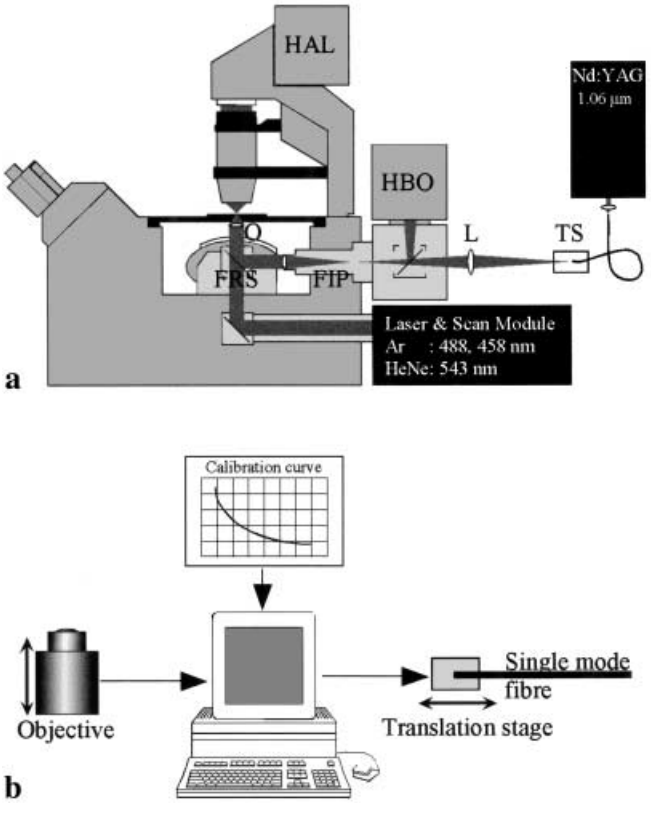

Fig. 1a,b. Experimental set-up. **a** Integration of the Nd:YAG laser used for optical tweezers in the LSM 510. **b** Synchronization of axial objective movement and movement of optical tweezers

1.2 Calibration

Calibration curves were determined for the oil-immersion objectives Zeiss Plan-Neofluar 100 × /1.3 oil and 63 × /1.25 oil (Carl Zeiss Jena GmbH, Jena, Germany). We used a dielectric mirror with high reflectance at 1064 nm (Laser Optik GmbH, Garbsen, Germany) placed like a cover glass. The signal emerging from the laser light used for optical tweezers that is reflected by the mirror was confocally detected with the scanning lasers turned off. Figure 2a schematically shows the optical path of the laser-tweezers system (components as described in Fig. 1a) and the confocal imaging system. The imaging system consists of a dichroic mirror ("M"), transmitting the light of the scanning lasers coming from below (not shown) and reflecting the signal coming from above, and a convex lens focusing the signal on the pinhole ("P") placed in front of the detector ("D"). In spite of the dielectric mirror in the fluorescence reflector slide ("FRS") being highly

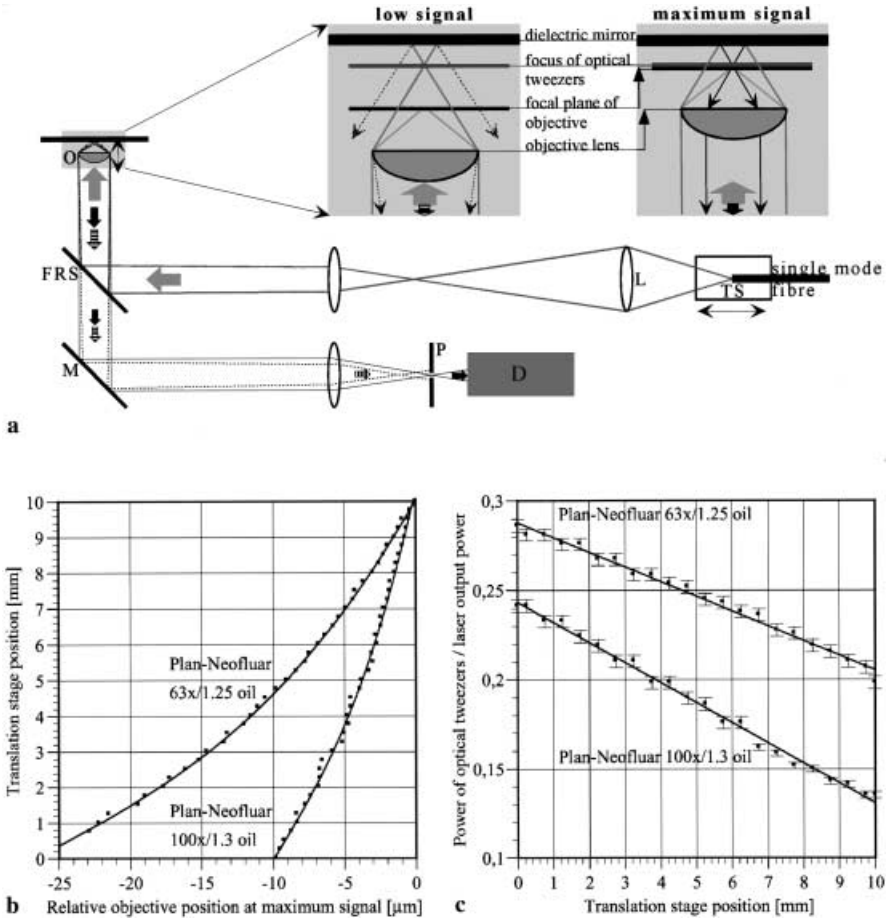

Fig. 2a–c. Calibration. **a** Schematic illustration of the laser-tweezers system and the imaging system. **b** Translation-stage position as a function of the relative objective position at maximum signal intensity for the objectives Plan-Neofluar 100 × /1.3 oil (*lower curve*) and 63 × /1.25 oil (*upper curve*) **c** Power of the laser light used for the optical tweezers emerging from the objectives Plan-Neofluar 100 × /1.3 oil (*lower curve*) and 63 × /1.25 oil (*upper curve*) as a function of the translation-stage position

reflective at 1064 nm, the reflection signal reaching the detector was sufficient using a laser power of about 140 mW to 290 mW and 110 mW to 170 mW emerging from the 100× and 63× objective, respectively. Figure 2a shows a particular position of the translation stage that results in a divergent laser beam entering the back aperture of the objective. The situation for two different axial objective-lens positions is illustrated by a solid and a dotted line and pointed out in the two figures showing an enlarged view of the field including the objective lens and the dielectric mirror. In the left-hand view, due to the divergent beam, the focus of the optical tweezers is situated above the focal plane of the objective. Because the reflected signal (dotted lines) is coming from out of the focal plane, the pinhole suppresses this signal. In the right-hand view the objective lens is shifted, placing the reflected focus of the optical tweezers (solid lines) in the focal plane of the objective. Here the signal is focused onto the pinhole resulting in a maximum signal.

The power of the optical tweezers emerging from the objective was recorded by placing a power meter (407 A, Spectra Physics, Darmstadt, Germany) just behind the particular objective close to its focus.

1.3 Fluorescent microspheres

Fluorescent microspheres with a diameter of 15 µm (variation of bead diameter < 3%) (FocalCheck F-7237, Molecular Probes via Mo Bi Tec, Göttingen, Germany) were used as test objects. These polystyrene beads are ring-stained, i.e., only their surface is stained by a dye, combined with a second fluorescent color throughout the bead. We used only the surface stain that was excited with the 488-nm line of the argon-ion scanning laser. Fluorescence was detected above 505 nm using a long-pass filter. For microscopy the microspheres were suspended 1 : 10 in distilled water with a final concentration of about 50 beads/µl. A drop of several microliters was put on a cover glass and covered by a small cap to prevent evaporation. The microspheres were trapped at a power of the optical tweezers of about 100 mW to 200 mW.

We determined the ring dimension of the individual cross sections of a microsphere with the software LSM 510 2.01 (Carl Zeiss Jena GmbH, Jena, Germany) using the profile function. This function displays the intensity in an optical section along an individually drawn straight line. Drawing this line across a ring through its center, two intensity maxima can be seen. The distance between these maxima was taken as the ring dimension. To reduce the random error accompanying this kind of determination, the ring dimension was determined by drawing the line four times across each ring through its center, each line forming an angle of 45° with the former line.

1.4 Elodea densa

Elodea densa (Canadian waterweed) was commercially obtained. For investigations with the CLSM, individual leaves

were freshly excised from a plant and mounted between two cover glasses with some tap water. Quiet cells were directly illuminated by the halogen lamp ("HAL" in Fig. 1a) to induce or accelerate their cytoplasmic streaming. For confocal imaging the chloroplasts were excited with the 488-nm line of the argon-ion scanning laser and showed an autofluorescence detected with a long-pass filter above 505 nm. Trapping of the chloroplasts was done using a power of the optical tweezers of about 100 mW to 200 mW. With this power no cell damage was observed.

1.5 AR42J cells

AR42J cells (ATCC, Manasses, USA) were cultivated at 37 °C and 5% CO_2 in RPMI medium with 10% FCS (SIGMA, Deisenhofen, Germany). For microscopy, cells grew on cover glasses under the same conditions for two up to five days. Staining was performed with cSNARF-AM (Molecular Probes via Mo Bi Tec, Göttingen, Germany) at a concentration of 10 μg/ml in RPMI medium without FCS. After incubation over 5 to 15 min the cells were rinsed with RPMI medium without FCS. Staining and microscopy were performed in a thermostat (Bachofer, Reutlingen, Germany) at 37 °C. Fluorescence was excited using the 488-nm and 543-nm lines of the scanning lasers. Emission was detected with two band-pass filters (565–595 nm, 625–656 nm).

2 Results

2.1 Compensated motion of the focus of the optical tweezers

For the 3D imaging of objects fixed by optical tweezers we started with the following approach: by varying the distance between the fiber end fixed on the motorized translation stage and lens "L", by moving the fiber end along the optical axis (see Sect. 1.1 and Fig. 1a for more details), the divergence of the beam entering the back aperture of the objective is changed. In this way the focus of the optical tweezers can be effectively shifted perpendicular to the focal plane (along the *z*-axis). This allows the compensation of an axial focal-plane motion by a simultaneous reverse motion of the focus of the optical tweezers in such a way that a trapped object maintains positioned on its intended position in the specimen.

For the realization of this approach it is necessary to determine a calibration curve giving the translation-stage position as a function of the axial objective position in such a way as to maintain the trapping position of the optical tweezers when the objective is moved. This was done using a dielectric mirror highly reflective at 1064 nm as a specimen reflecting the laser light used for optical tweezers (see Sect. 1.2 and Fig. 2a for more details). Here, using *z*-sectioning in laser scanning mode the *z*-position of the objective showing the optical section with the maximum intensity of the reflected signal was determined for different stage positions with an average accuracy of ±250 nm. On these particular objective positions the focus of the optical tweezers was situated in the focal plane of the objective (see Fig. 2a: maximum signal). The results are displayed in Fig. 2b showing the stage positions as a function of the determined relative objective positions at maximum signal intensity for the objectives Plan-Neofluar 100 × /1.3 (lower curve) and Plan-Neofluar 63 × /1.25 (upper curve). The highest relative objective positions at the stage position 10 mm are arbitrarily set to zero. With increasing stage position (increasing distance between fiber end and lens "L" in Fig. 1a) the objective position at maximum signal is nonlinearly shifted upward, meaning that the focus of the optical tweezers is shifted downward twice the distance of the objective shift due to reflection. Thus, multiplying the relative objective position in Fig. 2b by a factor of 2 reveals the final calibration curve giving the translation-stage position that maintains the focus position of the optical tweezers as a function of the relative axial objective position. Hence, a compensation of an objective motion to maintain the relative axial focus position of the optical tweezers appears possible over a *z*-distance of about 20 μm for the 100× objective and of about 50 μm for the 63× objective, restricted by the travel length of the translation stage. Since different objects are held at slightly different heights with respect to the focus of the optical tweezers [19, 20], the zero point of the calibration curve will finally be given at the stage position where the center of a particular trapped object is placed in the focal plane of the objective. The particular zero position can be simply adjusted within the developed controlling program.

Besides this, we determined the power of the laser light used for optical tweezers emerging from the objective as a function of the stage position (see Sect. 1.2). Figure 2c shows the power of the optical tweezers given in percent of the laser-output power for the 100× objective (lower curve) and the 63× objective (upper curve). Obviously, a linear relationship exists between the power of the optical tweezers and the stage position, being maximum at the smallest distance between the fiber end and the external lens. Thus, trapping efficiency decreases with increasing stage position, i.e., when the focus of the optical tweezers is shifted downward.

Furthermore, to compensate the axial focal-plane motion, the actual *z*-position of the objective has to be available without delay at any time. Otherwise the trapped object is still moving with the focus of the optical tweezers when the next optical section is scanned during *z*-sectioning. We could calculate the actual relative objective position from the signals controlling the motor that shifts the microscope objective (for more details see Sect. 1.1 and Fig. 1b). Although translation-stage motion starts almost immediately with axial objective motion (after about 20 ms), the final stage position is reached some 100 ms after objective positioning is completed. Since this time lag is situated in the time lag between the recording of two optical slices during *z*-sectioning, it has no visible effect.

2.2 Test of the compensation

Surface-stained microspheres with a diameter of 15 μm were used as test objects. When a drop of these polystyrene beads suspended in distilled water was put on a cover glass, the beads dropped onto the surface within a few minutes. It turned out to be hard to trap them once they were situated on the cover-glass surface. So they were trapped by turning on the optical tweezers when a bead, moving to the cover glass, reached a position shortly under the final trapping position. Above this position the bead was pushed away as radiation pressure countered the restoring force from the intensity gradient. Due to the surface stain (see Sect. 1.3), these beads,

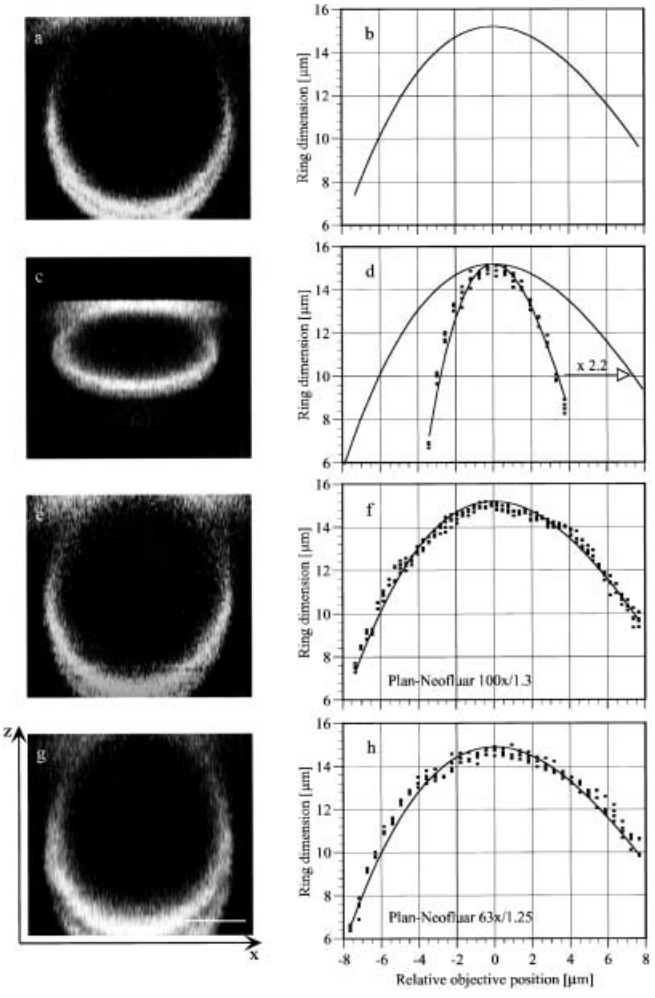

Fig. 3a–h. Compensation test with 15-µm microspheres. **a** $x-z$ view of an individual microsphere lying on the cover-glass surface in water (Plan-Neofluar 100 × /1.3 oil, 1024 × 1024 pixels, interval 300 nm). **b** Reference curve: Dependence of the ring dimension of the cross section ($x-y$ views) on the relative objective position. Data from four microspheres, taken as the microsphere in **a** , were averaged and fitted by a polynomial of third order. **c** $x-z$ view of a microsphere trapped by the optical tweezers using the lower curve of Fig. 2b (Plan-Neofluar 100 × /1.3 oil, 1024 × 1024 pixels, interval 450 nm). **d** Ring dimensions (*dots*) of the cross sections ($x-y$ views) of the microsphere in **c** as a function of the relative objective position compared with the reference curve of **b** (*solid line*). Each diameter was determined four times and the data are fitted by a polynomial of third order. **e** Same as **c**, but using lower curve of Fig. 2b multiplied by a factor of 2.2 (interval 300 nm). **f** Same as **d**, but ring dimensions of the microsphere in **e**. **g** Same as **c**, but using the upper curve of Fig. 2b multiplied by a factor of 2.5 (Plan-Neofluar 63 × /1.25 oil, scale bar 5 µm). **h** ring dimensions of the microsphere in **g** compared with the reference curve of the 63 × /1.25 oil objective

when viewed in cross section ($x-y$ view) with the CLSM, appeared as fluorescent rings of varying dimensions depending on the focal-plane position. Using z-sectioning a typical vertical view ($x-z$ view) of an individual bead situated on the cover-glass surface in water is shown in Fig. 3a. The second ring appearing in the lower part of this view is caused by a beam splitter the fluorescence signal has to pass through. We determined the ring dimensions of the individual cross sections as a function of the relative objective position as explained in Sect. 1.3. After averaging the data from four different microspheres the curve shown in Fig. 3b was obtained. Zero position is given at the objective position with maximum ring dimension, i.e., at the ring center. This curve and the $x-z$ view in Fig. 3a represent the reference used for the z-sectioning of microspheres trapped by the optical tweezers. For this we started with the objective Plan-Neofluar 100 × /1.3 oil using the lower curve shown in Fig. 2b. The $x-z$ view obtained from a z-sectioning of a microsphere trapped at a distance of about 20 µm to 30 µm from the cover-glass surface is shown in Fig. 3c. Compared with the reference in Fig. 3a it clearly appears compressed in the z-direction due to ignoring the multiplication factor 2. The determined ring dimensions as a function of the relative objective position together with the reference curve are shown in Fig. 3d. Comparing both it turns out that a multiplication factor of about 2.2 instead of 2 would have been relevant under the particular conditions. Equivalently, a factor of about 2.5 turned out for the objective Plan-Neofluar × 63/1.25 oil (results not shown). Considering these new factors to get the final calibration curves, the results obtained for microspheres trapped by the optical tweezers are shown in Fig. 3e–h: Figs. 3e and 3g show $x-z$ views taken with the 100× and 63× objectives, respectively. The respective ring dimensions as a function of the relative objective position together with the reference curves are shown in Figs. 3f and 3h. Now the $x-z$ views of the trapped microspheres and the determined ring dimensions match well with the reference ones over the z-dimension of 15 µm that could be tested with the microspheres.

2.3 CLSM imaging of moving chloroplasts of Elodea densa

We imaged chloroplasts (5 µm to 10 µm in diameter) in leaf cells of Elodea densa (Canadian waterweed) in order to demonstrate the optical tweezers for the 3D imaging of moving objects in cell biology. The cell cytoplasm containing the chloroplasts is limited to a thin layer surrounding a large central vacuole. Cytoplasmic streaming is seen in most cells as a cyclic movement along the cell walls with streaming rates of up to 12 µm/s [21]. It has been known for a long time that visible light can accelerate the cytoplasmic streaming in the cells that are illuminated directly [22]. We used this effect to induce or accelerate a vigorous cytoplasmic streaming in quiet cells (see Sect. 1.4).

Due to long image formation times of up to several seconds in laser-scanning mode, the chloroplasts following the vigorous cytoplasmic streaming could not be imaged without motional blurring as shown in Fig. 4a, using a scan time per frame of 15.7 s (1024 × 1024 pixels, average 2). With the optical tweezers an individual moving chloroplast could be fixed and shifted to the chloroplast-free cell center for undisturbed imaging, as shown in Fig. 4b. Using the optical tweezers for 3D imaging, Fig. 4c shows several optical sections of a trapped chloroplast spaced at z-intervals of 450 nm.

2.4 Dislocation of zymogen granules in AR42J cells

Pancreatic acinar cells are the starting point of pancreatitis, the self-digestion of the pancreas, and sometimes of pancreatic cancer. The cells possess zymogen granules (ZGs) containing proenzymes that get acidified to maintain the inactivity of the proenzymes and change their subcellular localization during a maturation process [23, 24]. To examine

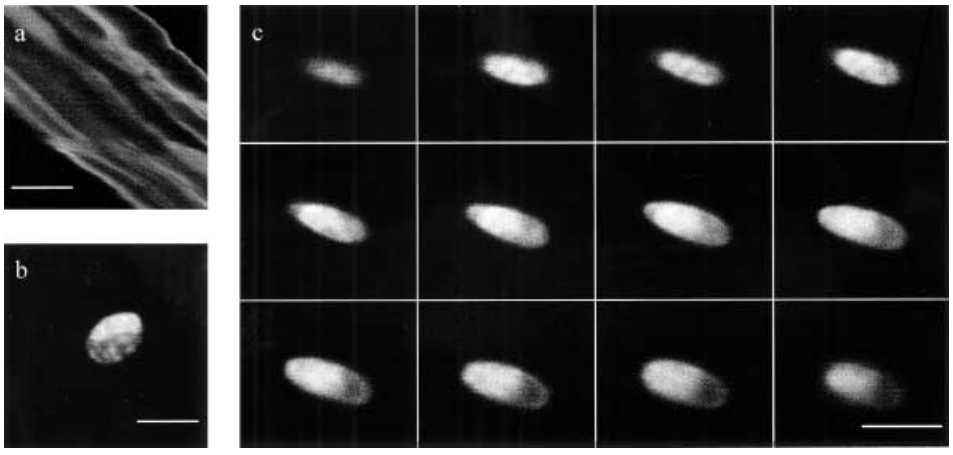

Fig. 4a–c. CLSM imaging of chloroplasts of Elodea densa. **a** A group of chloroplasts moving vigorously in the cytoplasmic streaming (1024 × 1024 pixels, scan time 15.7 s). **b** A single chloroplast fixed by the optical tweezers (1024 × 1024 pixels, scan time 15.7 s). **c** Cross sections ($x-y$ views) of a chloroplast fixed by the optical tweezers with a z-spacing of 450 μm (512 × 512 pixels, scan time per frame 1.9 s). (Plan-Neofluar 100 × /1.3 oil, scale bars 5 μm)

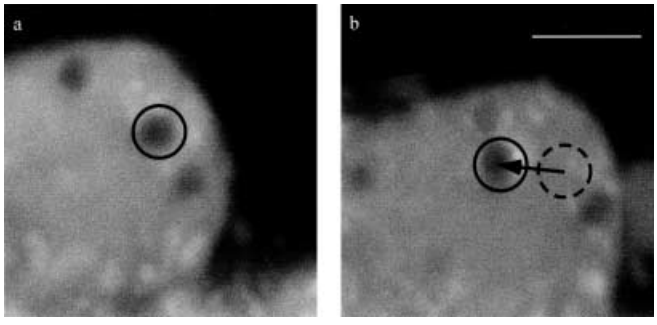

Fig. 5a,b. Displacement of zymogen granules (ZGs) in AR42J cells by optical tweezers. **a** A part of an AR42J cell with three visible ZGs, one marked by a ring. **b** The marked ZG after dislocation as indicated by rings and an arrow. (Plan-Neofluar 100 × /1.3 oil, 1024 × 1024 pixels, scale bar 5 μm)

the regulation of the ZG acidification in AR42J cells, derived from pancreatic acinar cells [25], as a function of the ZG position in the cell, we started to dislocate ZGs by the optical tweezers and to observe intracellular pH with the dye cSNARF-AM in the CLSM. Figure 5 shows the dislocation of an individual ZG in an AR42J cell using a power of the optical tweezers of about 120 mW. Because the optical tweezers is always located in the frame center, the specimen has to be moved for the dislocation of the trapped ZG. Thus, the cell appears shifted with respect to the frame after ZG displacement in Fig. 5b. The observable morphology change during displacement has to be the subject of further experiments to distinguish between effects caused by the light used for the optical tweezers and displacement effects.

The compensated motion of the focus of the optical tweezers will be necessary in future studies for the correct positional information of the ZG at subcellular level before and after dislocation.

3 Discussion

The experimental set-up presented here expands the field of applications of optical tweezers in confocal laser scanning microscopy. It is now possible to image objects three-dimensionally, such as chloroplasts in a cytoplasmic streaming, without distortion due to object movement during the image-acquisition time. In other applications optical tweezers can exert a tension on objects to maintain a dislocation while these objects are three-dimensionally imaged by the laser scanning microscope, for example in studies on the effects of intracellular microenvironment on organelle shape.

An alternative attempt to solve the problem of the movement of the focus of optical tweezers during three-dimensional image acquisition in CLSMs has been published in the literature [16, 17]. Here, in an inverted CLSM, an additional high numerical aperture objective placed opposite to the imaging one has been used to focus the laser used for the optical tweezers into the specimen. In this way the optical paths of the confocal imaging system and the laser tweezers system are completely separated and the two devices can operate independently. A disadvantage is the limited specimen thickness of about 50 μm due to the rapidly degrading quality of the confocal imaging, and degrading trapping efficiency of the optical tweezers with increasing penetration depth in the specimen arising from spherical aberration [16, 26, 27]. Furthermore, the use of devices like a microinjection apparatus or a thermostat is strongly restricted or even impossible because the specimen has to be placed between two cover glasses when using an oil-immersion objective as additional objective. These problems are not relevant with our set-up where the imaging lasers of the laser scanning microscope and the laser used for the optical tweezers are focused independently using the same objective lens.

The test of the compensation using surface-stained microspheres resulted in a multiplication factor of the calibration curve differing from the theoretical factor 2. Factors of 2.2 and 2.5 for the Plan-Neofluar objectives 100 × /1.3 oil and 63 × /1.25 oil, respectively, turned out to be relevant. This is because we only studied the focus position of the optical tweezers using a mirror for the determination of the calibration curves. Actually, the axial trapping position of an object in the optical tweezers is relevant and should be studied. This was done by using surface-stained microspheres as test objects. However, the trapping position can be influenced by different factors. For example, a changing distance between the focus of the optical tweezers and its trapping position is most likely when the focus of the optical tweezers is shifted perpendicularly to the focal plane of the objective. Another problem ignored using a mirror for the calibration arises from optical effects such as spherical aberration. Spherical aberration is induced by mismatches in the refractive index between cover glass and mounting medium, resulting in paraxial rays are focused differently from peripheral ones.

The result is a blurring of the intensity distribution of the focal region. Furthermore, the focus is situated closer to the cover glass [27, 28]. Hence, leaving the cover-glass surface results in a loss of resolution, intensity, and a focal shift. This affects the confocal imaging [15, 16] as well as the optical tweezers [17] and its trapping position. First studies with microspheres trapped by the optical tweezers without compensation showed a change of the axial position of a trapped microsphere with respect to the focal plane of the objective, when the penetration depth was increased (results not shown). Here, spherical aberration may have affected the trapping position of the optical tweezers differently from the focal-plane position of the objective due to the different wavelengths used, depending on the penetration depth in the specimen. Because this observation may have the consequence of calibration curves being dependent on the penetration depth, the effect of spherical aberration will be the subject of future studies. Since different objects have different shapes and optical properties resulting in different trapping positions in the optical tweezers, it further will have to be tested if they need separate calibration curves.

Acknowledgements. We gratefully acknowledge the financial support of the Bundesministerium für Bildung, Wissenschaft, Forschung und Technologie BMBF (grant No. AZ 11672) and of the Carl Zeiss Jena GmbH (Jena, Germany). We further wish to thank Dr. R. Wendenburg and R. Wolleschensky (Carl Zeiss Jena GmbH, Germany) for technical support as well as Dr. L. Wollweber (IMB Jena) for ideas and discussions and B. Lanick (IMB Jena) for cultivating the cells.

References

1. K.O. Greulich, J. Wolfrum: Ber. Bunsen-Ges. Phys. Chem. **93**, 245 (1989)
2. K.O. Greulich, J. Wolfrum: SPIE **1225**, 174 (1990)
3. M.W. Berns, W.H. Wright, R. Wiegand Steubing: Int. Rev. Cytol. **129**, 1 (1991)
4. K.O. Greulich, U. Bauder, S. Monajembashi, N. Ponelies, S. Seeger, J. Wolfrum: Labor **2000**, 36 (1989)
5. R. Wiegand Steubing, S. Cheng, W.H. Wright, Y. Numajiri, M.W. Berns: Cytometry **12**, 505 (1991)
6. K.O. Greulich: *Micromanipulation by Light in Biology and Medicine: The Laser Microbeam and Optical Tweezers* (Birkenhäuser, Basel, Wien, Boston 1999)
7. A. Pralle, E.-L. Florin, E. Stelzer, J.K.H. Hörber: Single Mol. I, **2**, 129 (2000)
8. A. Ashkin, J.M. Dziedzic, T. Yamane: Nature **330**, 769 (1987)
9. R.M. Simmons, J.T. Finer, S. Chu, J.A. Spudich: Biophys. J. **70**, 1813 (1996)
10. M.D. Wang, H. Yin, R. Landick, J. Gelles, S.M. Block: Biophys. J. **72**, 1335 (1997)
11. A. Kusumi, Y. Sako, T. Fujiwara, M. Tomishige: Methods Cell Biol. **55**, 173 (1998)
12. H. Felgner, F. Grolig, O. Müller, M. Schliwa: Methods Cell Biol. **55**, 195 (1998)
13. A. Ashkin, J.M. Dziedzic: Proc. Natl. Acad. Sci. USA **86**, 7914 (1989)
14. G. Leitz, G. Weber, S. Seeger, K.O. Greulich: Physiol. Chem. Phys. Med. NMR **26**, 69 (1994)
15. M.W. Berns, W.H. Wright, B.J. Tromberg, G.A. Profeta, J.J. Andrews, R.J. Walter: Proc. Natl. Acad. Sci. USA **86**, 4539 (1989)
16. K. Visscher, G.J. Brakenhoff: Cytometry **12**, 486 (1991)
17. K. Visscher, G.J. Brakenhoff, J.J. Krol: Cytometry **14**, 105 (1993)
18. A. Ashkin, J.M. Dziedzic: United States Patent Number 4 893 886 (16 Jan. 1990)
19. T. Wohland, A. Rosin, E.H.K. Stelzer: Optik **102**, 181 (1996)
20. A.D. Mehta, J.T. Finer, J.A. Spudich: Methods Cell Biol. **55**, 47 (1998)
21. J. Forde, M.W. Steer: Can. J. Bot. **54**, 2688 (1976)
22. L.V. Heilbrunn, F. Weber: *Protoplasmotologia Band VIII* (Springer, Wien 1959)
23. P.M. Motta, G. Macchiarelli, S.A. Nottola, S. Correr: Microsc. Res. Tech. **37**, 384 (1997)
24. V. Iwanji, J.D. Jamieson: J. Cell Biol. **95**, 734 (1982)
25. J. Christophe: Am. J. Physiol. **266**, G963 (1994)
26. S. Hell, G. Reiner, C. Cremer, E.H.K. Stelzer: J. Microsc. **169**, 391 (1993)
27. J.B. Pawley: *Handbook of Biological Confocal Microscopy* (Plenum, New York, London 1995)
28. P.C. Ke, M. Gu: J. Mod. Opt. **45**, 2159 (1998)